Environmental Earth Sciences (2018) 77:494
https://doi.org/10.1007/s12665-018-7690-1

ORIGINAL ARTICLE

Effects of rainfall infiltration and hysteresis on the settlement of shallow foundations in unsaturated soil

Sangseom Jeong[1] · Yongmin Kim[2] · Hyundo Park[1] · Jaehong Kim[3]

Received: 19 May 2017 / Accepted: 27 June 2018

Abstract
The effects of rainfall infiltration and hysteresis on the settlement of shallow foundations in unsaturated soil were numerically investigated. Numerical solutions were verified against experimental data. Rainfall intensities and groundwater table positions, factors that contribute to an additional settlement of shallow foundations, were investigated through a series of parametric studies. The effect of hysteresis on the settlement behavior of shallow foundations was considered by incorporating hysteretic soil–water characteristic curves (SWCC) that were obtained from the laboratory. A Reasonably good agreement of load-settlement response and matric suction distribution was obtained between the numerical analysis results and the field measurements. The parametric study showed that a reduction of matric suction due to rainfall infiltration induced the additional settlement of shallow foundations in unsaturated soil. The groundwater table position appeared to affect the wetting-induced settlement during rainfall due to the changes in matric suction. In addition, wetting SWCC analysis produced a slight larger settlement, up to 5% more than that produced by drying SWCC. Therefore, appropriate SWCCs (i.e., drying or wetting) should be used in numerical analysis in accordance with the conditions of the soils underneath the shallow foundations.

Keywords Infiltration · Shallow foundation · Settlement · Unsaturated soil · Numerical analysis

Introduction

Shallow foundations have been situated on unsaturated soils, ignoring the existence of matric suction that is closely related to the shear strength of the soil (Rojas et al. 2007; Vanapalli and Mohamed 2007; Jeong et al. 2008; Kim et al. 2016; Wu and Selvadurai 2016). Settlement is important in foundation engineering and might be affected by matric suction in accordance with the principles of unsaturated soil mechanics. However, the design of shallow foundations is conducted in accordance with the principles of saturated soil mechanics.

A considerable number of researchers have studied the effects of matric suction on the strength of unsaturated soil. Rahardjo et al. (2011) proposed an empirical equation to estimate the modulus of elasticity with the incorporation of matric suction. They concluded that the soil stiffness appears to increase with increasing matric suction. Oh et al. (2009) also developed a theoretical equation for the modulus of elasticity with respect to matric suction that incorporated the soil–water characteristic curve (SWCC). Nevertheless, past research has neglected the effect of matric suction, which leads to an overestimation of the settlement of shallow foundations. Very few studies have attempted to examine the transient behavior of unsaturated soil in inducing additional settlement of shallow foundations through laboratory or model tests. The main influencing factors on the fundamental mechanism of the settlement behavior of shallow foundations were investigated (Briaud and Gibbens 1999; Oh and Vanapalli 2011; Mohamed 2014). Numerical studies were also carried out to estimate the settlement of shallow

✉ Yongmin Kim
kimkimym@ntu.edu.sg

Sangseom Jeong
soj9081@yonsei.ac.kr

Hyundo Park
park-0809@yonsei.ac.kr

Jaehong Kim
woghd@dsu.ac.kr

[1] School of Civil and Environmental Engineering, Yonsei University, Seoul, South Korea

[2] School of Civil and Environmental Engineering, Nanyang Technological University, Singapore, Singapore

[3] Department of Civil Engineering, Dongshin University, Naju, South Korea

Published online: 02 July 2018

foundations under steady-state and transient conditions (Abed and Vermeer 2009; Park 2017). However, while these previous studies were focused on the effect of matric suction, few studies have examined the effect of rainfall infiltration on shallow foundation stability because of the difficulties associated with the determination of the input parameters in constitutive equations and the uncertainties associated with the flux boundary conditions.

Unsaturated soils below shallow foundations usually experience wetting–drying cycles due to climate conditions. The wetting–drying cycles have a significant impact on SWCCs (Fredlund and Rahardjo 1993). Hysteresis may affect the mechanical behavior and transient process in unsaturated soils (Nuth and Laloui 2008; Rahardjo et al. 2013; Kim et al. 2016). However, the effect of hysteresis has also been ignored in assessing the settlement of shallow foundations. In particular, no study has been carried out on the investigation of hysteresis for simulations of a shallow foundation under rainfall.

In this study, the effects of rainfall infiltration and hysteresis on the settlement of shallow foundations in unsaturated soil were numerically investigated. Numerical solutions were compared with experimental data for verification. Rainfall intensities and groundwater table positions that contribute to the additional settlement of shallow foundations were investigated through a series of parametric studies. The effect of hysteresis on the settlement behavior of shallow foundations was considered by incorporating hysteretic SWCCs obtained from the laboratory. Index properties and hysteretic SWCCs of the Dogye weathered granite soil were used for numerical analyses. The nonlinear relationship between the modulus of elasticity and matric suction was considered in the sequential analysis. In combination with numerical results, these observations give insight into the effects of rainfall infiltration and hysteresis on the settlement behavior of shallow foundations in unsaturated soils.

Numerical modeling of unsaturated soil

Modulus of elasticity

During rainfalls, unsaturated soil can become saturated and may lose all of its additional strength because negative pore-water pressure that contributes additional shear strength increases to zero or to positive values. Therefore, it is necessary to incorporate not only the shear strength but also the modulus of elasticity of the soil to assess the settlement of shallow foundations. Oh et al. (2009) performed model tests for sand under different matric suctions to investigate the load-settlement behavior of model footing. They developed a theoretical equation to evaluate the modulus of elasticity for unsaturated soil with respect to matric suction using the modulus of elasticity for saturated soil, SWCC, and using fitting parameters (α and β) as follows:

$$E_{i(\text{unsat})} = E_{i(\text{sat})}\left[1 + \alpha \frac{u_a - u_w}{p_a/101.3} S^{\beta}\right] \quad (1)$$

where $E_{i(\text{unsat})}$ and $E_{i(\text{sat})}$ are the initial tangent modulus elasticity under unsaturated and saturated conditions, respectively, p_a is the atmospheric pressure, and S is the degree of saturation. In Eq. 1, α and S^{β} control the nonlinear variation of the modulus of elasticity. The term $p_a/101.3$ is used for maintaining consistency with respect to the dimensions and units. In this study, Eq. 1 was used to evaluate the modulus of elasticity for unsaturated soil with the fitting parameters $\alpha = 0.04$ and $\beta = 0.8$.

Negative pore-water pressure

Variations in negative pore-water pressure with depth can be calculated using the initial groundwater table position and the maximum negative pore-water pressure head. It was assumed that the negative pore-water pressure varies hydrostatically with respect to the initial groundwater table, as shown in Fig. 1. If the maximum negative pressure head, H_{max}, is lower than the height of the unsaturated soil layer, H_{unsat} (i.e., $H_{\text{max}} < H_{\text{unsat}}$), then the negative pore-water pressure is constant up to the ground surface beyond the maximum negative pressure head. On the other hand, if the maximum negative pressure head is greater than the height of the unsaturated soil layer (i.e., $H_{\text{max}} > H_{\text{unsat}}$), then the negative pore-water pressure increases hydrostatically up to the ground surface.

Cohesion and dilatancy angle

For sands, the internal frictional angle is not influenced by matric suction (Vanapalli et al. 1996; Wang et al. 2002). However, Hossain and Yin (2010) demonstrated that the

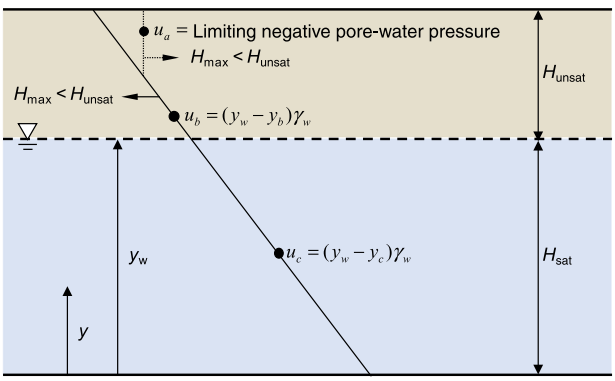

Fig. 1 Modeling of pore-water pressure using PLAXIS 2D software

dilatancy angle of unsaturated soils increased with increasing matric suction. However, there was a lack of sufficient observations to explain the entire mechanics of dilatancy angle of unsaturated soil. Bolton (1986) proposed an equation for the friction angle for sand in an unsaturated condition as

$$\phi' = \phi'_{\text{crit}} + 0.8\psi_p \tag{2}$$

where ϕ' and ϕ'_{crit} are the effective internal friction angle under given and critical conditions, respectively, and ψ_{p} is the peak dilatancy angle, which is $3.75I_{\text{R}}$ for the triaxial condition. I_{R} is the dilatancy index that can be expressed by

$$I_{\text{R}} = I_{\text{D}}\left[Q + \ln\left\{\frac{p_{\text{a}}}{100P'_{\text{p}}}\right\}\right] - 1 \tag{3}$$

where I_{D} is a relative density that varies from 0 to 1, Q is the intrinsic soil variable, and P'_{p} is the peak mean effective stress. ϕ'_{crit} is often deemed to be a constant for sand. An increasing dilatancy angle means an increasing friction angle. Therefore, ϕ'_{crit} represents variations in the dilatancy angle with respect to the friction angle.

Hysteretic soil–water characteristic curve

Laboratory experiments were conducted using the apparatus of Wayllace and Lu (2012) for measuring the hysteretic soil–water characteristic curve (SWCC). The apparatus can measure the drying process as well as the wetting process by controlling the air pressure applied to a saturated soil specimen, as shown in Fig. 2. The tests took approximately 22–40 days for the initial drying and main wetting processes for the weathered granite soil in Korea.

A weathered granite soil sampled from the Dogye area in Korea was selected for the experiment. The specimen was prepared from reconstituted weathered granite to minimize difficulties associated with soil heterogeneity. Laboratory tests were conducted to estimate the index properties of the specimen. The optimum water content, as determined by the Proctor compaction test, was 13.7%, corresponding to a maximum dry unit weight of 17.5 kN/m^3 in the Dogye weathered granite soil. The procedure for preparing soil specimens included drying the soil using the oven, crushing the soil particles, passing the soil particles through a 2 mm sieve, and then mixing the sieved soil particles with the amount of water required to reach a specific water content. The soil was then wrapped in polyethylene bags and stored at constant temperature and humidity for 48 h to reach equilibrium. Index properties of weathered granite soil are summarized in Table 1.

Hysteretic SWCCs represent different volume fractions of water under the same matric suction between drying and wetting processes. This is attributed to the ink-bottle effect, the pore-fluid contact-angle, and the swelling and shrinking of the soil structure. Figure 3 shows the experimental result of the SWCC for Dogye weathered granite soil and curves fitted with the van Genuchten (1980) equation. Hydraulic

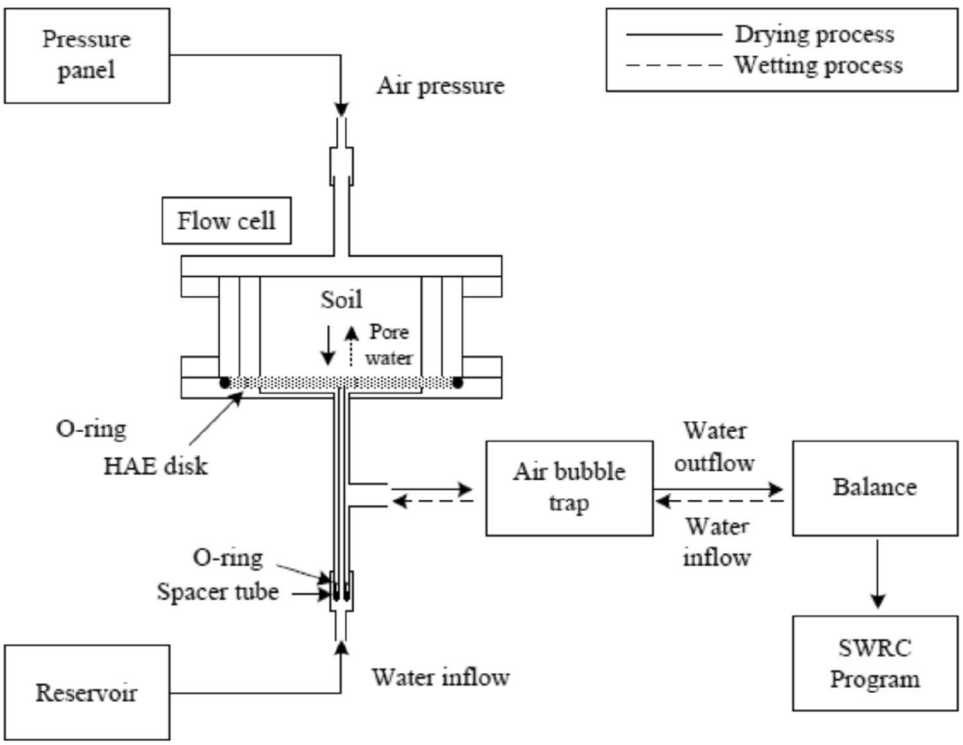

Fig. 2 Schematic diagram of the apparatus for soil–water characteristic curve tests

Table 1 Index properties of Dogye weathered granite soil

Index properties	Value
Maximum dry unit weight, $\gamma_{d,max}$ (kN/m^3)	17.5
Minimum dry unit weight, $\gamma_{d,min}$ (kN/m^3)	13.5
Saturated hydraulic conductivity, k_s (m/s)	4.76×10^{-7}
Coefficient of uniformity, C_u	9.27
Coefficient of gradation, C_c	1.47
Specific gravity, G_s	2.72
Plastic limit, PL (%)	12.17
Plastic index, PI (%)	16.18
USCS classification	SW

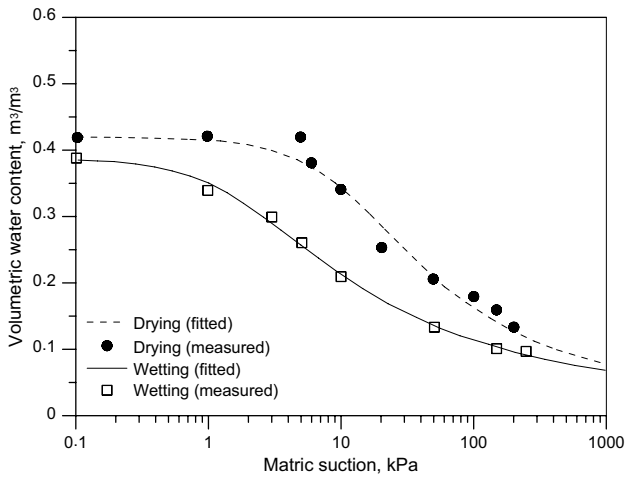

Fig. 3 Hysteretic soil–water characteristic curves for Dogye weathered granite soil

Table 2 Soil–water characteristic curve fitting parameters predicted by van Genuchten (1980)

Index property	Drying SWCC	Wetting SWCC
Saturated volumetric water content, θ_s	0.418	0.387
Residual volumetric water content, θ_r	0.032	0.032
Degree of saturation, S_r (%)	0.077	0.083
Fitting parameter, α (1/kPa)	0.042	0.643
Fitting parameter, n	1.469	1.353
Fitting parameter, m	0.319	0.261

properties and fitting parameters of the SWCCs for the soil are summarized in Table 2.

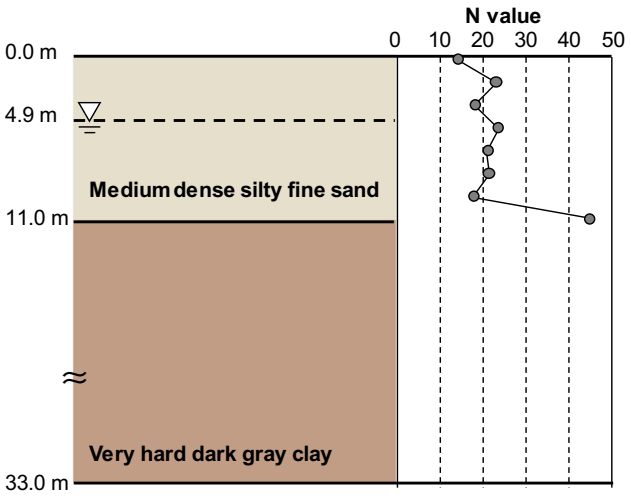

Fig. 4 In-situ soil profile at load test site (Modified from Briaud and Gibbens 1999)

Validation

Field load tests of shallow foundations

Field load tests of shallow foundations on unsaturated soils (Briaud and Gibbens 1999) were simulated to verify the finite element (FE) model. A comprehensive field and laboratory study was carried out to obtain in-situ soil properties. Four different sizes (i.e., 1.0×1.0 m^2, 1.5×1.5 m^2, 2.5×2.5 m^2, and 3.0×3.0 m^2) of shallow foundations were modeled in unsaturated sand.

Figure 4 shows the in-situ soil profile and the average standard penetration test (SPT) values per 0.3 m performed near the footings. The SPT values indicated that the upper soil layer at a depth of 11 m is medium dense silty sand and that the lower soil layer at a depth of 33 m is very hard dark gray clay. The soil layers contained between 2–8 and 5–30% fine materials at the 3 m depth and 9 m depth, respectively. According to the Unified Soil Classification System (USCS), the in-situ soil was classified as silty sand (SM). Grain-size distribution curves with depth and the index properties of soils based on the site investigations are shown in Fig. 5 and Table 3, respectively.

A two-dimensional (2D) axisymmetric condition was used to model four different sizes of shallow foundations and unsaturated soils. A commercial finite element computer program, PLAXIS 2D (2012), was used for the numerical analysis. The unsaturated soils were considered to be under drained conditions during the loading stage. The overall dimensions of the model boundaries comprised a width of 30 m and a depth of 18 m. The outer boundary of the model was fixed against displacements (Fig. 6).

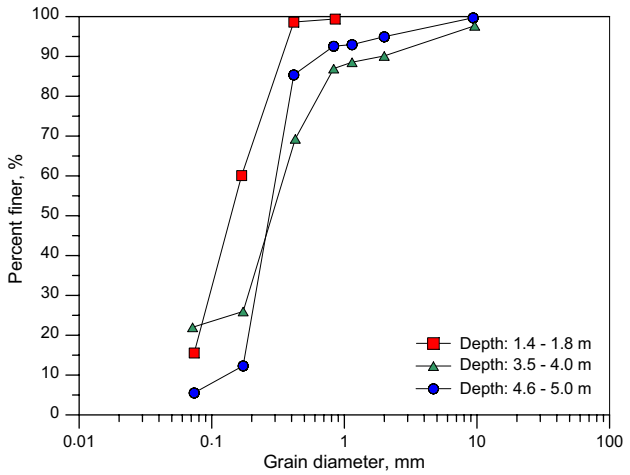

Fig. 5 Grain-size distributions (Modified from Briaud and Gibbens 1999)

Table 3 Index properties of in-soil (Briaud and Gibbens 1999)

Soil property	Value
Unity weight, γ_t (kN/m^3)	17.75
Water content, w (%)	5.0
Specific gravity, G_s	2.64
Void ratio, e	0.78
USCS	SM

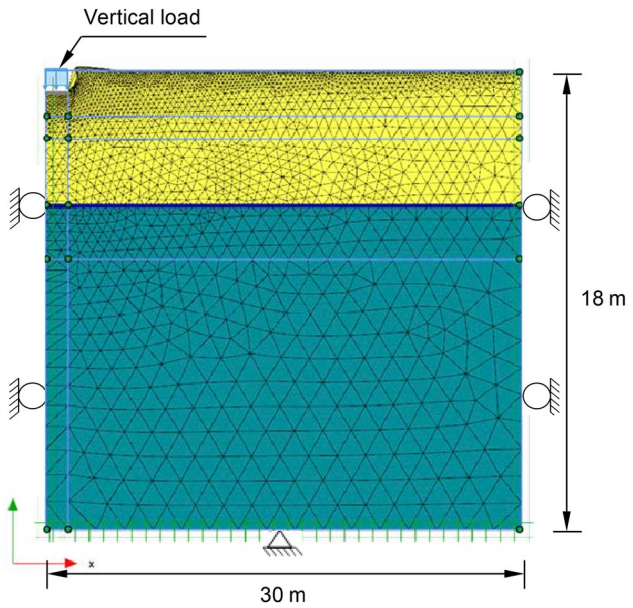

Fig. 6 Finite element model and displacement boundary condition for simulating field load tests

Table 4 Material properties used in numerical analysis

Soil property	Value
Modulus of elasticity of soil, $E_{i(\text{unsat})}$ (MPa)	45
Modulus of elasticity of footing, E_{footing} (MPa)	10,000–70,000
Poisson's Ratio, ν	0.3
Effective internal friction angle, ϕ' (deg)	35
Effective cohesion, c' (kPa)	1
Dilation angle, ψ (deg)	26

The mesh consisted of 15-node triangular elements. The linear-elastic model for the foundation and the Mohr–Coulomb model using the non-associated flow rule for sand were used for the finite element model. The effective cohesion (c'), effective internal friction angle (ϕ'), and dilation angle (ψ) of the sand were assigned to the Mohr–Coulomb model. The modulus of elasticity ($E_{i(\text{unsat})}$) of unsaturated soil was inferred from Eq. 1 using the fitting parameters of 0.04 for α and 0.8 for β. The material properties used in the numerical analysis are summarized in Table 4.

The initial equilibrium condition is important in the numerical analysis. The specified initial stress distributions should be matched with a calculation of the self-weight of the foundation. Two construction stages were required for the stability analysis of shallow foundations. First, the foundation was placed on the unsaturated soil layer by applying the force of gravity. Next, after equilibrium was reached, the applied load was simulated by the application of a vertical distribution load at the top of the shallow foundation. Note that the shallow foundation was assumed to be in a stress-free state at the beginning of the analysis to ignore the effect of the installation.

Figure 7 presents the comparison of load-settlement responses between numerical and measured results for different sizes of shallow foundations. The results indicate reasonably good agreement with those obtained from the field load tests. A stiffer load-settlement response was observed in the case of the 1.5 × 1.5 m^2 shallow foundation than in the numerical results. The settlement of shallow foundations in unsaturated soil depended on the types of soil and water content. Although the numerical model cannot rigorously simulate complicated in-situ conditions, the mode results followed the general trend of measured load-settlement responses.

A higher settlement was observed in the case of the 3.0 × 3.0 m^2 shallow foundation than in those of the relatively lower dimensions, as shown in Fig. 7d. Several researchers have studied size effects on settlement. Briaud (2007) proposed a method to account for size effects by plotting applied stress versus the normalized settlement curves (i.e., δ/B). The Federal Highway Administration (1997) concluded that the stress–strain behaviors of the samples

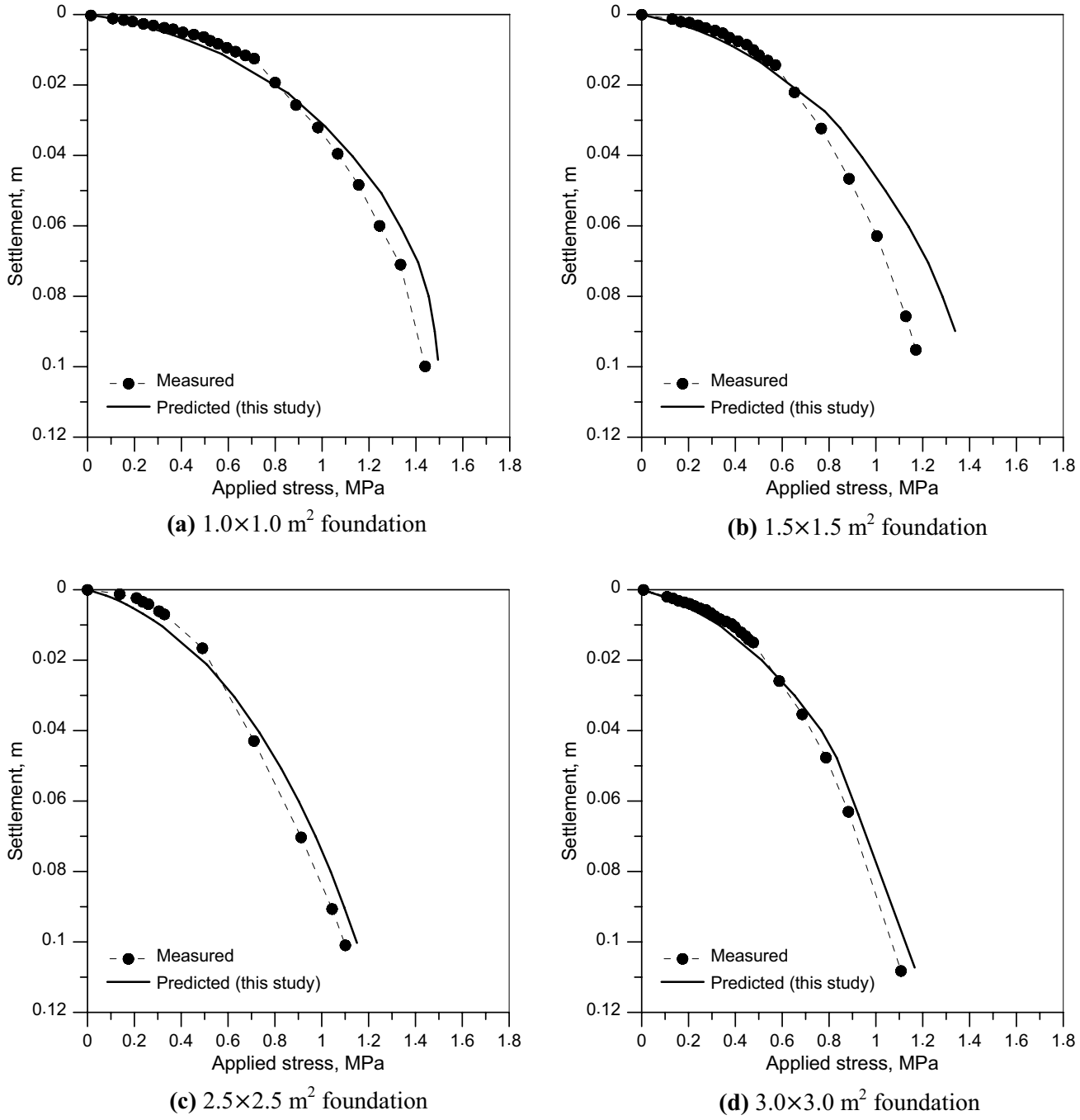

(a) 1.0×1.0 m^2 foundation

(b) 1.5×1.5 m^2 foundation

(c) 2.5×2.5 m^2 foundation

(d) 3.0×3.0 m^2 foundation

Fig. 7 Comparison of load-settlement curves between numerical and measured results

are unique regardless of the sample diameter when triaxial tests are carried out for identical sand samples under the same confining pressure. Consoli et al. (1998) also reported uniqueness of the normalized curves under the homogeneous and isotropic condition of sites. Based on the literature, the size effect on the shallow foundation was ignored in this study.

Field matric suction

Flow analysis results were compared with on-site measurements to predict distributions of matric suction. Figure 8 shows that field measurements were carried out in the longitudinal direction along the watershed. Matric suction was measured at a total of six locations (T1–T6), and a total of

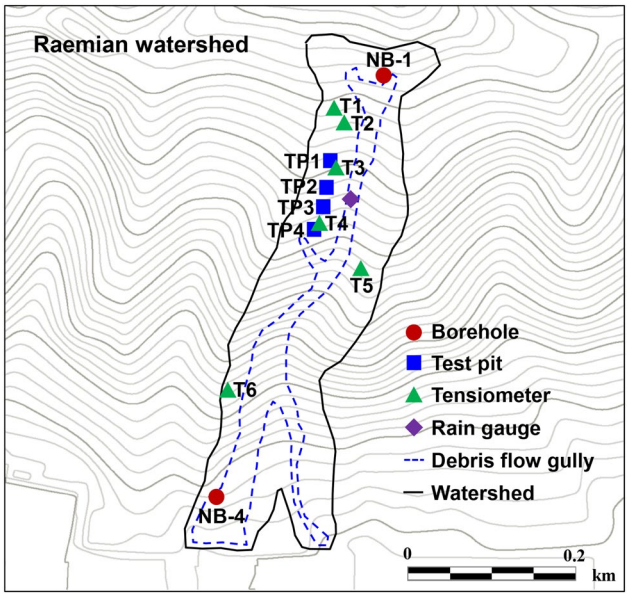

Fig. 8 Location of soil investigation and matric suction monitoring in Raemian watershed (Kim et al. 2016)

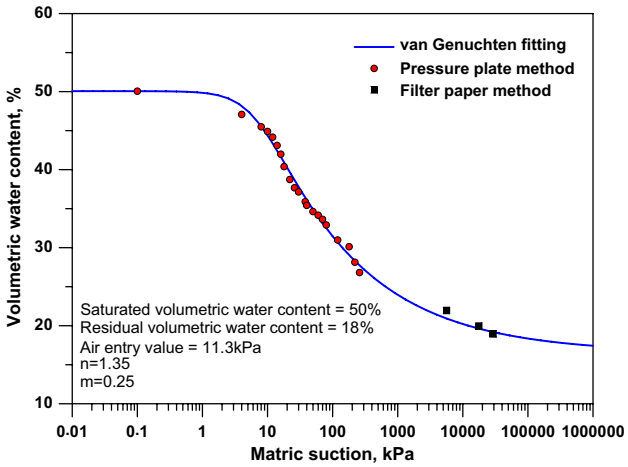

Fig. 9 Soil–water characteristic curve of colluvium in Raemian watershed (Kim et al. 2016)

18 tensiometers were installed (Kim et al. 2016). Laboratory experiments were carried out on collected on-site samples to analyze index properties. SWCC variables were estimated using the graphical method shown in Fig. 9. The input parameters used in the analysis are summarized in Table 5. Rainfall conditions applied to the analysis are based on the real-time rainfall measurements at the time of the event.

Furthermore, representative results of T1 were chosen for the comparison. Figure 10 shows the field matric suction distribution at 30, 60, and 130 cm depths with dashed lines and the simulated matric suction at the same depth with

Table 5 Model parameters used in numerical analysis (Kim et al. 2016)

Soil property	Value
Saturated volumetric water content, θ_s	0.61
Residual volumetric water content, θ_r	0.17
Saturated permeability, k_s (m/s)	8.0×10^{-7}
Fitting parameter, α (1/kPa)	11.3
Fitting parameter, n	1.35
Fitting parameter, m	0.25

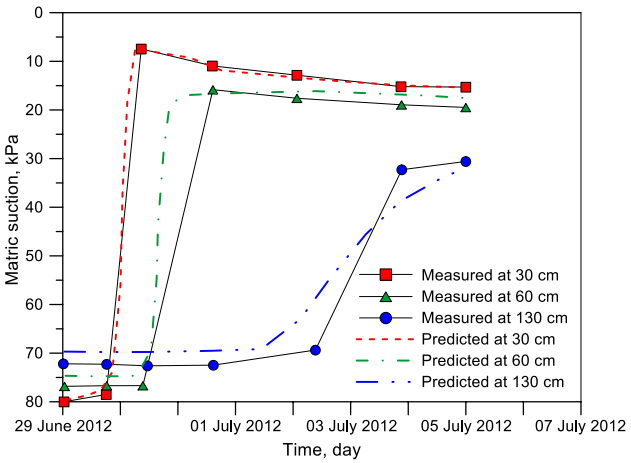

Fig. 10 Comparison of matric suction between numerical and measured results

solid lines. After rainfall on 30 June 2012, the matric suction quickly decreased to 6 kPa. Over an extended period of time, the residual matric suction became 20 kPa. The matric suction at 0.6 and 1.3 m also decreased, although the effect was delayed and less significant because of the greater depth.

Meanwhile, a lower matric suction was observed in the upper 0.3 m of the soil than in the lower layers, corresponding to a higher water content in the upper layer. Lower matric suction resulted in higher unsaturated permeability, which allows greater downward infiltration of rainwater and indicates the possible formation of preferential local seepage. The comparisons confirm that the simulation can describe the distribution of field matric suction with satisfactory accuracy.

Infiltration analysis of shallow foundation in unsaturated soil

FE model and input parameters

A 2D FE model to simulate the response of a shallow foundation subjected to rainfall infiltration in unsaturated soil

using PLAXIS 2D (2012) is presented. Figure 11 shows the typical FE mesh for the simple circular shallow foundation and shows the applied displacement boundary conditions. The mesh extended to a distance of 10*B* beyond the center of the shallow foundation and to a depth of 5*B* beneath the shallow foundation, where *B* (=5.0 m) is the foundation width. The boundary dimensions were found to be sufficient to prevent boundary effects. Poulos and Davis (1974) reported that stress is primarily transferred to the ground in the 0–1.5*B* depths; therefore, the groundwater table position is assumed to be at both 1*B* and 2*B* below the ground surface.

Dogye weathered granite soil was selected for the parametric studies. The drying and wetting SWCCs tested from the laboratory were used, as shown in Fig. 3. The mechanical and hydraulic properties of the Dogye weathered granite soil are summarized in Tables 1 and 2, respectively. The hysteresis effect (e.g., drying and wetting processes) was considered in the numerical analysis. Figure 11 shows applied flux boundary conditions for transient seepage analyses. Rainfall intensities of 10, 20, and 30 mm/h with durations of 96 h were applied to the ground surface; no ponding was allowed to prevent hydrostatic pressure from the ground surface. The left and right edges above the groundwater table were specified as no flow boundaries ($Q = 0$). The FE model from the ground surface to 5*B* below had a mesh size of approximately 0.75 m to obtain accurate results within the infiltration zone. Two independent sequential analyses were performed using PLAXIS 2D (2012), as shown in Fig. 12. First, a rainfall flow analysis was conducted with the incorporation of unsaturated hydraulic properties to estimate the distribution of matric suction due to rainfall infiltration. Second, a deformation analysis was conducted with the incorporation of the Young's modulus inferred from the specified matric suction. Table 6 summarizes the combination of factors for parametric studies.

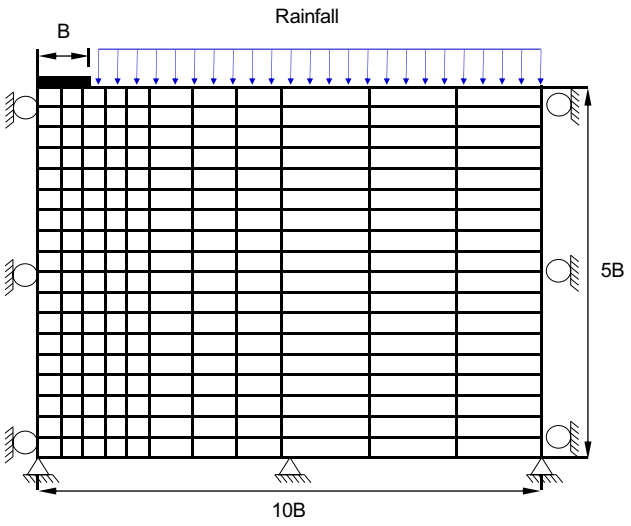

Fig. 11 Finite element model and boundary conditions for parametric study

Load-settlement curve during rainfall

Figure 13 shows the load-settlement curves of the 5 × 5 m^2 shallow foundation subjected to a rainfall intensity of

Table 6 Cases of parametric studies

Soil type	Foundation size	Groundwater table positions	Rainfall intensities (mm/h)	Rainfall durations (h)
Dogye weathered granite soil	5 × 5 m^2	1*B*	10	1
		2*B*	20	12
			30	24
				48
				96

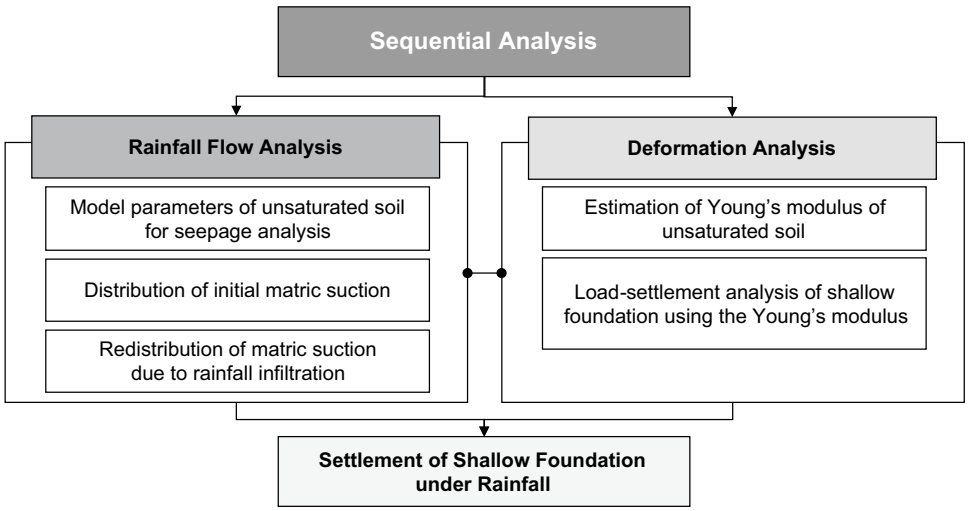

Fig. 12 Flow chart of the sequential analysis

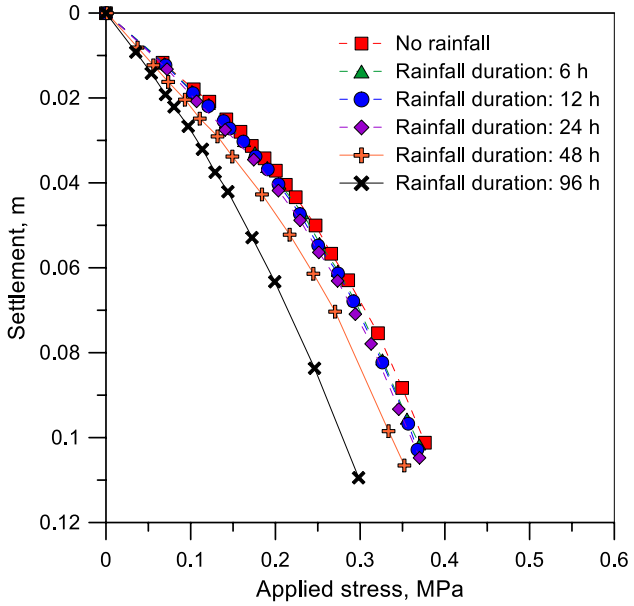

Fig. 13 Load-settlement curves of 5 × 5 m^2 foundation under rainfall intensity of 10 mm/h and groundwater table 2B below

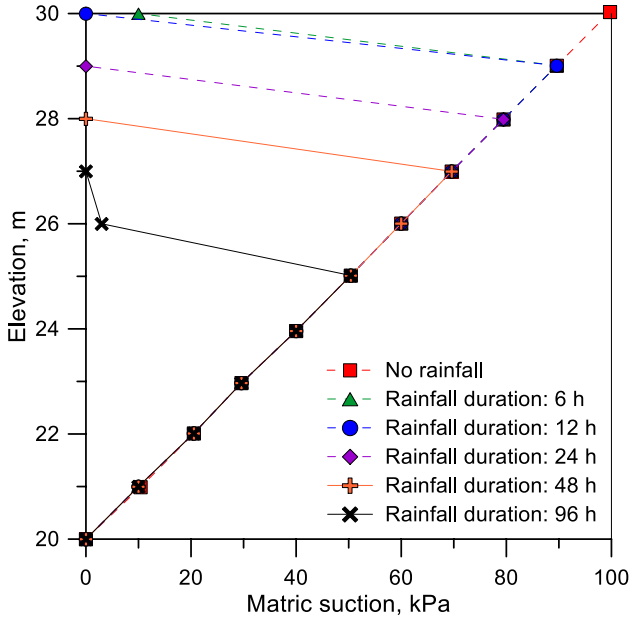

Fig. 14 Matric suction distributions of the 5 × 5 m^2 shallow foundation under a rainfall intensity of 10 mm/h and groundwater table 2B below

10 mm/h with the groundwater table 2B below. The initial slope of the load-settlement curves decreased continuously with time, resulting in a bearing capacity reduction for the shallow foundation. The bearing capacity of the shallow foundation significantly dropped after 48 h due to prolonged rainfall. The decrease in bearing capacity could be attributed to the settlement that occurred during the first two days and that then accelerated until the soil became saturated. Figure 14 shows matric suction distributions during rainfall for the soil. Matric suction gradually decreased with an increase in rainfall duration. After 48 h, matric suction rapidly decreased, resulting in decreases in bearing capacity. Rainwater infiltration into specific depths was closely dependent on the permeability of the soil. The matric suction at each time step was used for the evaluation of the modulus of elasticity and for the corresponding settlement in the deformation analysis.

Settlement during rainfall

Figure 15 shows the variations in the settlement of shallow foundations with respect to rainfall intensities (10, 20 and 30 mm/h) and groundwater table positions (1B and 2B) in the Dogye weathered granite soil under a constant stress of 170 kPa. The results show that rainfall infiltration contributed to an increase in the settlement of the shallow foundation due to the reduction of matric suction above the groundwater table. The settlement under the groundwater table 2B below increased gradually when rainfall intensities escalated, and the rate of additional settlement appeared to be affected by the rainfall intensities. In contrast, the settlement under the groundwater table 1B below increased rapidly and the rate of additional settlement was significant compared to those of the groundwater table 1B below. This finding could be attributed to the initial matric suction that governs the infiltration rate of the soil. The modulus of elasticity of unsaturated soils with respect to different matric suction distributions was incorporated in the numerical analysis. It was also found that the groundwater table near the ground surface induced a larger additional settlement than the deeper groundwater table.

Effect of hysteresis during rainfall

Figure 16 shows variations in the settlement of shallow foundations in Dogye weathered granite soil with wetting SWCC under a constant stress of 170 kPa. The general trend of settlement was similar to the results of the drying SWCC. However, the amount of settlement slightly increased to 5% compared to those of the drying SWCC. The settlement should be affected by the modulus of elasticity with respect to matric suction. At the same volumetric water content, the wetting SWCC exhibited lower matric suction compared to the drying SWCC. Consequently, the relatively smaller modulus of elasticity was considered in the analysis when the wetting SWCC was used, as shown in Fig. 17. Similar results about the effect of hysteresis on infiltration and shear strength in unsaturated soils were found by Goh et al. (2013). They concluded that

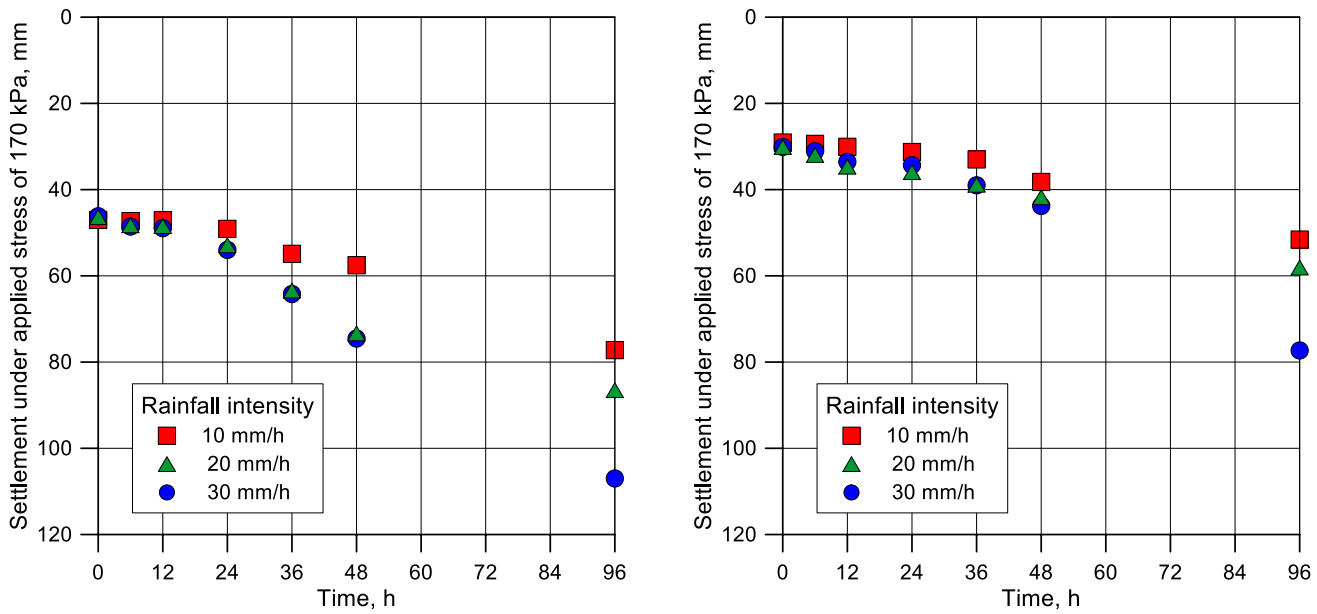

(a) Groundwater table 1B below **(b)** Groundwater table 2B below

Fig. 15 Variations in the settlement of shallow foundation under 170 kPa applied stress in Dogye weathered granite soil with drying SWCC

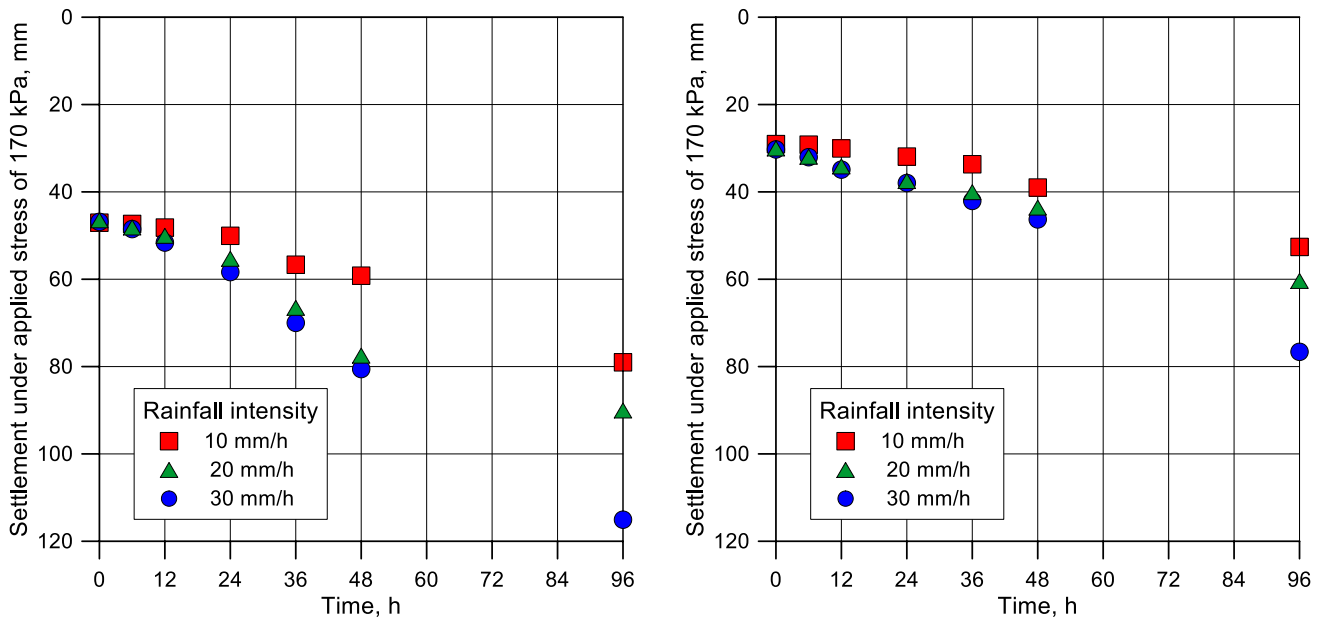

(a) Groundwater table 1B below **(b)** Groundwater table 2B below

Fig. 16 Variations in the settlement of shallow foundation under 170 kPa applied stress in Dogye weathered granite soil with wetting SWCC

sand-kaolin specimens on drying paths have higher shear strengths than those on wetting paths. Table 7 summarizes the settlement of the shallow foundation with respect to groundwater table positions and hysteretic SWCCs.

Conclusions

The effects of rainfall infiltration on the settlement of shallow foundations for unsaturated soil were numerically investigated using the finite element analysis commercial

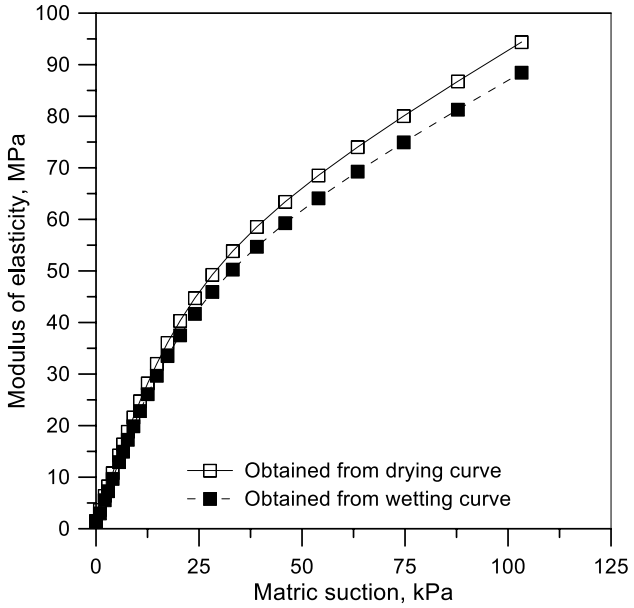

Fig. 17 Variation of modulus of elasticity with respect to matric suction for Dogye weathered granite soil

software PLAXIS 2D. The effect of hysteresis on the settlement behavior of shallow foundations was considered by incorporating hysteretic soil–water characteristic curves (SWCCs) obtained from the laboratory. The nonlinear relationship between the modulus of elasticity and matric suction was considered in the sequential analysis. The numerical solutions were validated against the experimental data. In addition, parametric studies were carried out to explore the factors affecting additional settlement of shallow foundations. The following conclusions can be drawn:

1. The analysis that incorporated matric suction found reasonably good agreement for load-settlement response between the numerical analysis and the field load test results. Moreover, the distribution of matric suction with different depths was well predicted by the developed 2D FE model.
2. The initial matric suction in unsaturated soil exhibited obvious reinforcing effects for the stability of shallow foundations as settlement decreased because of the high modulus of elasticity as the matric suction increases.
3. The settlement of shallow foundations in unsaturated soil was significantly influenced by rainfall intensity. The reduction of matric suction due to rainfall infiltration induced the additional settlement of shallow foundations. The variations in the groundwater table position near the ground surface during rainfall also affected the settlement behavior of shallow foundations because the lower position produced the higher initial matric suction based on unsaturated soil mechanics.
4. The analysis by the wetting SWCC produced up to 5% greater shallow foundation settlement compared to the drying SWCC. For rigorous analysis and design, therefore, the appropriate SWCCs (i.e., drying or wetting) should be employed in accordance with the conditions experienced by the soils underneath the shallow foundation.

Table 7 Summary of settlements for shallow foundation with respect to groundwater table positions and hysteretic SWCCs

Time	Soil with drying SWCC (mm)			Soil with wetting SWCC (mm)		
	10 mm/h	20 mm/h	30 mm/h	10 mm/h	20 mm/h	30 mm/h
	Groundwater table 1B below					
0	46.98	46.31	46.13	46.99	46.45	46.81
6	47.25	48.22	48.52	47.28	48.09	48.46
12	47.04	48.40	48.90	48.11	50.00	51.55
24	49.05	52.84	53.94	50.00	55.26	58.31
36	54.84	63.36	64.17	56.62	66.49	69.94
48	57.48	73.29	74.49	59.13	77.44	80.52
96	77.17	86.46	106.95	78.97	90.00	115.01
	Groundwater table 2B below					
0	29.02	30.05	30.05	29.00	30.00	30.23
6	29.33	31.90	31.03	29.13	31.89	32.00
12	30.02	34.63	33.50	30.00	34.11	34.85
24	31.22	35.89	34.28	31.86	37.46	37.91
36	32.95	38.81	38.95	33.62	40.01	42.02
48	38.17	41.71	43.74	38.95	43.54	46.25
96	51.53	58.02	77.26	52.55	60.33	76.57

5. A framework for the modeling of unsaturated soil with sequential numerical analyses provided good understanding of the mechanism leading to wetting-induced instability of shallow foundations under transient conditions that lead to an additional settlement.

References

Abed AA, Vermeer PA (2009) Numerical simulation of unsaturated soil behaviour. Int J Comput Appl Technol 34(1):2–12

Bolton MD (1986) The strength and dilatancy of sands. Géotechnique 36(1):65–78

Briaud JL (2007) Spread footings in sand: Load settlement curve approach. J Geotech Geoenviron Eng 133:905–920

Briaud JL, Gibbens R (1997) Large scale load tests and data base of spread footings on sand. Technical report, FHWA–RD–068, US Department of Transportation Federal Highway Administration

Briaud JL, Gibbens R (1999) Behavior of five large spread footings in sand. J Geotech Geoenviron 125(9):787–796

Consoli NC, Schnaid F, Milititsky J (1998) Interpretation of plate load tests on residual soil site. J Geotech Geoenviron Eng 124:857–867

Fredlund DG, Rahardjo H (1993) Soil mechanics for unsaturated soils. John Wiley and Sons Inc., New York

Goh SG, Rahardjo H, Leong EC (2013) Shear strength of unsaturated soils under multi-cycles of drying and wetting. J Geotec Geoenviron Eng 140(2):1–5

Hossain MA, Yin JH (2010) Shear strength and dilative characteristics of an unsaturated compacted completely decomposed granite soil. Can Geotech J 47(10):1112–1126

Jeong S, Kim J, Lee K (2008) Effect of clay content on well-graded sands due to infiltration. Eng Geol 102:74–81

Kim Y, Jeong S, Kim J (2016) Coupled infiltration model of unsaturated porous media for steady rainfall. Soils Found 56(6):1073–1083

Mohamed FMS (2014) Bearing capacity and settlement behaviour of footings subjected to static and seismic loading conditions in unsaturated sandy soils. Dissertation, University of Ottawa

Nuth M, Laloui L (2008) Advances in modelling hysteretic water retention curve in deformable soils. Comput Geotech 35:835–844

Oh WT, Vanapalli SK (2011) Modelling the applied vertical stress and settlement relationship of shallow foundations in saturated and unsaturated sands. Can Geotech J 46(8):903–914

Oh WT, Vanapalli SK, Puppala AJ (2009) Semi-empirical model for the prediction of modulus of elasticity for unsaturated soils. Can Geotech J 48:425–438

Park HD (2017) Rainfall induced load-settlement behavior of shallow foundations on unsaturated soil. M.Sc. Thesis, Yonsei University, Seoul, Korea

PLAXIS 2D (2012) PLAXIS 2D user manual, version 2012, Brinkgreve, Swolfs RB, W.M., PLAXIS Inc

Poulos HD, Davis EH (1974) Elastic solutions for soil and rock mechanics. Wiley, New York

Rahardjo H, Melinda F, Leong EC, Rezaur RB (2011) Stiffness of a compacted residual soil. Eng Geol 120:60–67

Rahardjo H, Satyanaga A, Leong EC (2013) Effect of flux boundary conditions on pore-water pressure distribution in slope. Eng Geol 165:133–142

Rojas JC, Salinas LM, Sejas C (2007) Plate-load tests on an unsaturated lean clay. Experimental unsaturated soil mechanics. Springer, Berlin Heidelberg, pp 445–452

van Genuchten MT (1980) A closed-form equation for predicting the hydraulic conductivity of unsaturated soils. Soil Sci Soc Am J 44(5):892–898

Vanapalli SK, Mohamed FM (2007) Bearing capacity of model footings in unsaturated soils. Experimental unsaturated soil mechanics. Springer, Berlin Heidelberg, pp 483–493

Vanapalli SK, Fredlund DG, Pufahl DE, Clifton AW (1996) Model for the prediction of shear strength with respect to soil suction. Can Geotech J 33(3):379–392

Wang Q, Pufahl DE, Fredlund DG (2002) A study of critical state on an unsaturated silty soil. Can Geotech J 39(1):213–218

Wayllace A, Lu N (2012) A transient water release and imbibitions method for rapidly measuring wetting and drying soil water retention and hydraulic conductivity functions. Geotech Test J 35(1):103–117

Wu LZ, Selvadurai APS (2016) Rainfall infiltration-induced groundwater table rise in an unsaturated porous medium. Environ Earth Sci 75(2):1–11